P.20

NASA CONTRACTOR REPORT 189678

TENSION AND COMPRESSION FATIGUE RESPONSE OF UNNOTCHED 3D BRAIDED COMPOSITES

M. A. Portanova

Lockheed Engineering & Sciences Company
Hampton, VA

Contract NAS1-19000
AUGUST 1992

National Aeronautics and
Space Administration
Langley Research Center
Hampton, Virginia 23665-5225

Introduction

A research program was initiated to measure the fatigue response of a 3-D braided composite. Unnotched compression and tension fatigue response of a 3-D braid are reported. Post-impact and open hole fatigue specimens will be tested. Both gross compressive stress and tensile stress were plotted against cycles to failure to evaluate the fatigue life of these materials. Damage initiation and growth was monitored visually and by tracking loss of stiffness. The intent of this research is to establish by what means the strength of a 3-D architecture will start to degrade, at what point it will degrade beyond an acceptable level, and how this material will typically fail.

Test Specimens

The material tested is a [±30°/0°] multiaxial braid constructed from AS4/12K tow graphite fibers and BP E905L resin. The graphite tows were braided on a cylinder, in a single pass, at the desired thickness. The preform was the removed from the cylinder, slit down its length and then stitched along the cut edge to maintain the braid angle. The dry fabric preform was then resin transfer molded. All plates were cured in the same mold resulting in uniform fiber volume fraction and thickness. Fiber volume fraction averaged 52%. Thickness varied between 5.92 mm (0.233 in.) and 6.15 mm (0.242 in.). The average was 6.10 and 5.99 mm for the compression and tension specimens, respectively.

All specimens were machined with a diamond saw and all edges ground smooth and parallel. Because composites tend to be fairly notch sensitive, it was decided to machine a large radius in the test section of the unnotched specimens. The test section for both tension and compression specimens were reduced from an overall width of 38.1 mm (1.5 in.) to 25.4 mm (1.0 in.). An illustration of the tension and compression fatigue specimens is shown in Figure 1.

The compression fatigue specimens were mostly end loaded so only a minimal amount of material was inserted in the hydraulic grips. Accordingly, steel plates, approximately 0.762 mm (0.03 inch) thinner than the compression specimen, were placed in the grips. These plates are shown in Figure 2. The specimen ends bore on the plates inside the hydraulic grips. Only a minimal amount of clamping pressure was used. Thus, the coupons were mostly end loaded without brooming deformation of the ends of the specimens. The gauge length was kept short at 76.2 mm (3.0 in.) to prevent buckling/instability.

The tension fatigue specimens were clamped tightly in the hydraulic grips using approximately 3.45 MPa (5000 psi) grip pressure in order to transfer the load into the specimen through friction. The area of gripped surface was 1451.6 mm^2 (2.25 $in.^2$) to prevent crushing. To insure that the gage length was constant, the tension specimens were also seated on top of the steel plates illustrated in Figure 2. Photographs of the load frame, test specimens, and data acquisition system are provided in Figure 3.

Test Equipment and Methods

Fatigue tests were performed in a closed-loop servo-hydraulic testing machine in load-control mode. All testing was conducted at room temperature. The compression fatigue tests were run at a cyclic frequency of 10 Hz. The tension fatigue tests were cycled at only 5 Hz to maintain loading accuracy. Feedback error increased with increasing frequency. The testing machine had a cycle counter as well as a shut-off feature to halt testing at specimen failure or at some pre-determined cycle count. The compression tests were run at a stress ratio (minimum/maximum) of 10 while the tension tests were run with a stress ratio of 0.1.

Load cell, machine stroke and strain gage output were recorded using a digital storage oscilloscope that allowed dynamic measurements during the first cycle and then again at predetermined cycle counts during a test. These load-strain outputs were recorded in real time and stored on magnetic media. This data was later converted to stress-strain data and plotted. A linear least squares fit was then plotted against the zero to 3000 $\mu\varepsilon$ data. This process was repeated at various cycle counts throughout the fatigue life. This data was used to monitor the change in stiffness of the specimens as a result of damage growth. The surface of the specimen was visibly inspected to monitor the initiation and progression of damage in these materials.

Strain gages provide a measure of the strain field, averaged under the gage. With textile composites, the strains on the surface will vary within the unit cell of the fiber architecture, where unit cell refers to the smallest repeating geometry of the textile architecture. The gage must be larger than a unit cell to provide an accurate homogenization of the strain. The unit cell of this 3-D braid was calculated to be 8.636 mm (0.340 inch) in the 0° direction, 4.98 mm (0.196 inch) in the 90° direction, and 0.706 mm (0.0278 inch) through the thickness. Therefore, 12.7 mm (0.5 inch) long by 4.57 mm (0.18 inch) wide strain gages were used for the majority of the fatigue test. Some fatigue specimens were tested with 25.4 mm (1.0 inch) long by 6.35 mm (0.25 inch) wide, see table 1 & 2. For the monotonically loaded specimens, 6.35 mm (0.25 inch) long by 4.57 mm (0.18 inch) wide strain gages were used for the tension specimens and 3.175 mm (0.125 inch) long by 2.54 mm (0.10 inch) wide strain gages for the compression specimens. All specimens were tested with 0° strain gages while some fatigue specimens were tested with both 0° and 90° stacked gages. The effect of these various gage sizes will be discussed.

Fatigue Test Results

Compression Fatigue

Maximum compressive load is plotted against cycles to failure in Figure 4. The fatigue test results are listed in Table 1. The values plotted at one cycle are the static failure stresses from the room temperature short block compression tests which are also reported in Table 1. Linear least squares regression fits to the data are also plotted. The braids exhibited a wide range of fatigue lives for a fairly narrow range of cyclic stresses. This response is typical of that for tape materials of similar constituents. At 10^6 cycles, the strengths were 43 to 44% less than the static values.

Airframe manufactures typically design aircraft for a fatigue life of two lifetimes, where one lifetime is approximately 20 years or 60,000 flights. A design allowable of 0.004 strain has been suggested for tape laminates on the basis of damage tolerance. To evaluate the fatigue performance of the braided material, a region covering one to two lifetimes has been shaded and a dashed line placed at a $\frac{2}{3}$ x 0.004 strain level (limit condition), based on the materials initial modulus. At one lifetime, the fatigue strength is about 1.8 times the limit stress. For wing bending on a typical transport aircraft, the strains reach limit condition only a few times in a lifetime, which is much less than 60,000 cycles. Therefore this material, in an unnotched form, has more than adequate fatigue strength.

The notched static strength of the 3-D braid is about $\frac{3}{4}$ the unnotched strength. Assuming that the slopes of the notched and unnotched S-N curves are similar, the fatigue strength of the notched material may be marginal. Future open hole fatigue tests will

establish whether or not the braided material has adequate fatigue capability.

Tension Fatigue

Maximum tensile stress is plotted against cycles to failure in Figure 5. Results are also listed in Table 2. The values plotted at one cycle are the static failure stresses from the monotonic room temperature tension tests reported in Table 2. A polynomial curve was fit to the data. The 3-D braids experienced a reduction in tensile strength with constant amplitude tension fatigue cycles of between 21 and 22% at 10^6 cycles. For cycles less than 10^6, the strength reduction was much less than that for the compression fatigue data. The fatigue response of this material suggests that, although the off-axis yarns may delaminate or fail early in the life, the strength, being mostly dependent upon the 0° fibers, retains most of its initial value.

Again, a region representing one to two design lifetimes has been shaded and the design limit strain of $\frac{2}{3}$ x 0.004 is shown. The unnotched tension fatigue response of this material is more than adequate. The notched static tension strength is approximately 28% below the unnotched strength. Assuming that the slope of the S-N curve is similar, the notched fatigue response should also be more than adequate.

Damage Initiation and Progression

Because of the small distance between the hydraulic grips, it was not possible to obtain radiographs of the specimens without removing the specimens from the testing machine. Thus, damage was monitored visually and through stiffness loss curves. A more thorough description of damage initiation and progression will be

conducted in the future on this same material with both open holes and impact damage.

Compression Fatigue

Compliance change during cyclic loading provides a measure of damage accumulation. The specimen stiffness was monitored in situ throughout the fatigue life, including the fracture cycle with a digital storage scope. Figure 6 is a plot of the in situ elastic modulus normalized by the initial modulus versus the corresponding cycle count normalized by the number of cycles to failure for a typical high cycle, low cycle and run-out compression fatigue test.

In laminated composites, under monotonic compressive loading the epoxy tends to crack and delaminate prior to overall failure. In this material, matrix failure from fatigue loading was similar to that observed under static loading. Damage appeared to be very localized near the specimens edges on the front and back surfaces of the specimen. Matrix cracks formed in the resin rich areas along the braided tows, running the length of the tow at the surface of the specimen. These tows appeared to lose their ability to support load at this point because they buckled on each consecutive loading cycle. No damage was seen to grow through the thickness of the specimen at its edge. Postmortem inspection of the fracture surface showed that the fracture typically ran along the ±30° braid angle, sometimes passing under those tows crossing the fracture path and sometimes turning parallel to them. Final failure of the specimen was by shear kinking of the undamaged tows.

With the compression fatigue specimens, stiffness loss started early in the fatigue life but progressed very slowly. The material typically retained 96% of its original elastic modulus over 75% of its fatigue life. With high cycle fatigue, the stiffness can be seen to drop rapidly after about 75% of its life. Surface damage also developed very rapidly at this point. At failure, the loss of elastic modulus ranged

from 16 to 18.5%. With low cycle fatigue, the loss of elastic modulus ranged from 4.5 to 6% at failure. Surface damage was not observed during low cycle fatigue. Specimen runout (10^6 cycles) yielded a 1 to 3% reduction in modulus. Some edge surface damage was observed mid-way in the life but did not appear to grow across the width or through the thickness to any significant degree.

Tension Fatigue

Figure 7 is a plot of the in situ elastic modulus normalized by the initial modulus versus the corresponding cycle count normalized by the number of cycles to failure for a typical high cycle and low cycle fatigue test. Stiffness loss for a runout specimen was not measured. The tension fatigue specimens exhibited faster initial damage growth rates then the compression specimens. Visually, damage was not apparent on the specimens surface but was concentrated at the edge of the specimen. Figure 7 reveals an immediate loss of stiffness for both high and low cycle fatigue tests.

Early in the life, broken fibers and matrix cracks were observed between the braided tows on the edge of the specimen. It is believe that the broken fibers were artifacts of the machining process and were not indicative of fatigue failures. For the low cycle tension fatigue test, the average loss of elastic modulus ranged from 3% to 5% within the first 20% of the fatigue life. Edge damage was observed early in the life and seemed to propagate at a fairly constant rate.

With high cycle fatigue, edge damage again was observed early in the life but grew little there after. Examination of Figure 7 reveals that with high cycle fatigue the stiffness drops 6% to 8% during the first 20% of the fatigue life. Damage did not grow along the surface of the coupon until late in the fatigue life. Some edge damage was observed mid-way in the life but did not appear to grow across the

width or through the thickness to any significant degree until late in the life of the coupon.

Near final failure, damage consisted of matrix cracks between tows on the surface of the specimen adjacent to the edge damage. At failure, specimens for both high and low cycle tests retained 86% to 89% of their initial elastic modulus. Postmortem inspection of the specimens revealed fiber pullout and fractured fibers, along with severe matrix damage. The matrix cracks had run from the specimens free edge towards the center of the specimen, following the ± 30 braid angle.

Effect of Various Strain Gage Lengths

Figure 8 is a plot of the initial modulus versus strain gage size for the static and fatigue test; data scatter is also displayed with error bars. Strain gage sizes are given in Tables 1 & 2. Examination of this figure reveals that different strain gage sizes produced different elastic modulus values. Tension modulus was larger than compression modulus for each of the tested gage sizes. For static compression loading and 3.18 mm (0.125 inch) strain gages, the elastic modulus averaged 50.12 GPa (7.27 Msi.). For static tensile loading and 6.35 mm (0.25 inch) gages, the average elastic modulus was 63.98 GPa (9.28 Msi.). For compression fatigue loading and 12.7 mm (0.5 inch) and 25.4 mm (1.0 inch) strain gages, the elastic moduli were 65.08 Gpa (9.44 Msi) and 75.50 GPa (10.81 Msi) respectively. A textile composite is not a homogeneous material at the strain gage levels. Thus, the strains vary with gage size.

Of the gages used, the 3.18 mm (0.125 inch) gage, which is much smaller than one unit cell, yielded the lowest modulus values. The 6.35 mm (0.25 inch) gage, which is only slightly smaller than one unit cell, provided an average elastic modulus very similar to the values obtained with the 12.7 mm (0.5 inch) gages. Both the 6.35

mm (0.25 inch) and 12.7 mm (0.5 inch) gages provided average modulus values 30% larger than the 3.18 mm (0.125 inch) gages. The 25.4 mm (1.0 inch) gage, which is approximately 3 unit cells in length, yielded a modulus 49% larger than the 3.18 mm (0.125 inch) gage but only 14% larger than the 6.35 mm (0.25 inch) and 12.7 mm (0.5 inch) gage. The tension fatigue moduli had similar variations. For tension fatigue loading, 12.7 mm (0.5 inch) and 25.4 mm (1.0 inch) strain gages produced values of 74.73 GPa (10.70 Msi) and 84.09 GPa (12.04 Msi) respectively.

The specimen width varied along the length of these coupons. All stress calculations on the fatigue specimens were performed using the minimum cross-sectional area of the test section, i.e., one inch. The width varied less than 1.4% along the 25.4 mm (1.0 inch) strain gage length. Elastic moduli was also determined using the stroke output during the tension test. The average value determined using stroke output was 66.53 GPa (9.65 Msi). This value has very good agreement with the compression tests and 12.7 mm (0.5 inch) gages.

Summary

In general, the fatigue strength of the 3-D braided composite, in an unnotched form, is more than adequate. Tension fatigue strengths were greater than compression. Assuming that the slope of the S-N curve is similar for notched materials, the notched fatigue life should also be adequate for tension but perhaps marginal for compression. There was a larger loss in tension modulus with fatigue cycles than with compression modulus. Damage consisted of resin cracks within tows and resin rich areas. Modulus measurements with strain gages increased with gage length until gages were longer than unit cell size.

Specimen ID	% of P_{max}	Cycles to Failure	Maximum Stress, MPa σ_{max}	Maximum 0° Strain, % ε_{max}	Initial Modulus GPa E	In-situ Poisson's Ratio ν	Strain Gage Length & Orientation
STC**	100	1	446.78	1.038	50.12	0.757	.125,0°/90°
1	63.3	779,000	282.69	0.434	65.98	0.714	0.5, 0°/90°
2	67.3	79,400	300.61	0.494	60.95	---	0.5, 0°
3	71.8	3,440	320.61	0.495	64.53	---	0.5, 0°
4	65.9	328,770	294.41	0.463	63.85	---	0.5, 0°
5	61.3	612,330	273.72	0.359	67.91	0.728	0.5, 0°/90°
6	53.7	*3.1 E6	239.94	0.290	68.67	0.69	0.5, 0°/90°
7	57.3	*2.7 E6	255.80	0.316	74.53	---	1.0, 0°

Table 1. Compression Fatigue Test Results
* denotes runout
** static compression test

Specimen ID	% of P_{max}	Cycles to Failure	Maximum Stress, MPa σ_{max}	Maximum 0° Strain, % ε_{max}	Initial Modulus GPa E	In-situ Poisson's Ratio ν	Strain Gage Length & Orientation
STT**	100	1	681.41	1.075	63.98	0.997	.25,0°/90°
1	66.9	*2.8 E6	455.74	0.487	84.12	---	1.0, 0°
2	96.9	3,218	660.52	0.949	77.70	---	0.5, 0°
3	72.0	670,110	490.91	0.627	75.08	---	0.5, 0°
4	77.9	548,680	530.90	0.690	77.50	---	0.5, 0°
5	84.2	468,000	573.64	0.950	89.22	0.80	0.5, 0°/90°
6	91.2	46,800	621.22	0.945	73.57	0.80	0.5, 0°/90°
7	94.8	25,910	646.46	0.932	78.26	0.82	0.5, 0°/90°

Table 2. Tension Fatigue Test Results
* denotes runout
** static tension test

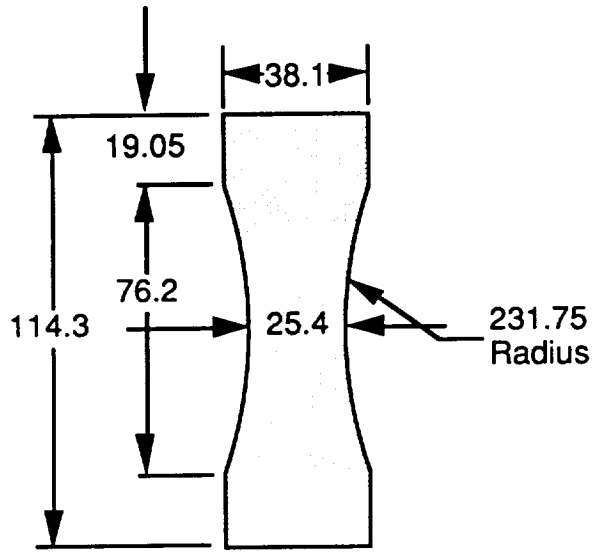

a) Compression

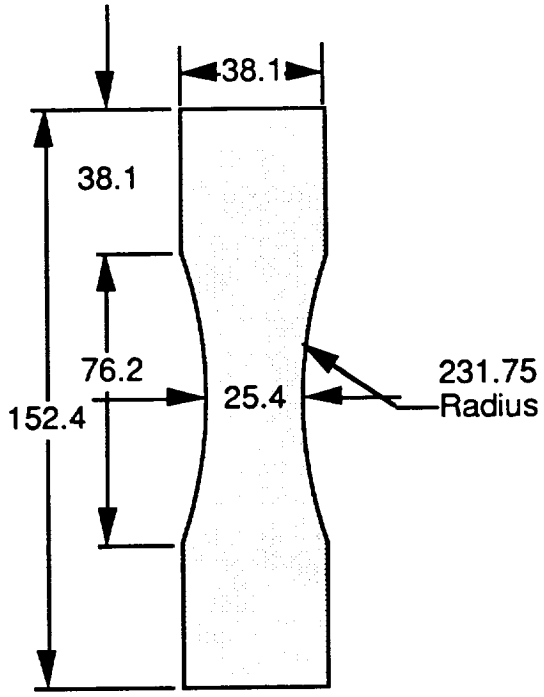

b) Tension

Figure 1. Fatigue Test Specimen Geometry.

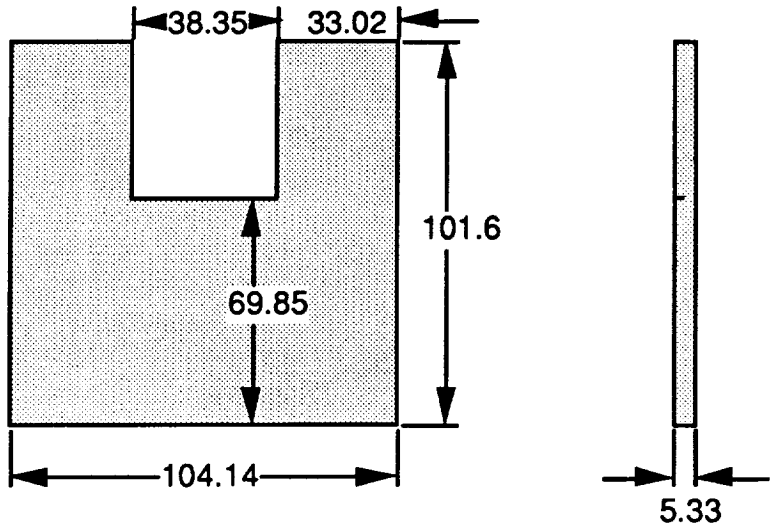

b) Tension

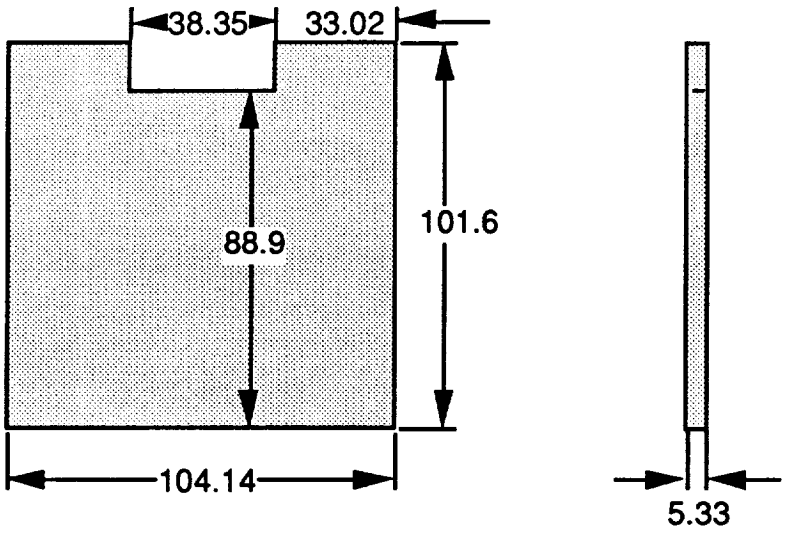

a) Compression

Figure 2. Dimensions for end loading plates used inside the hydraulic grips.

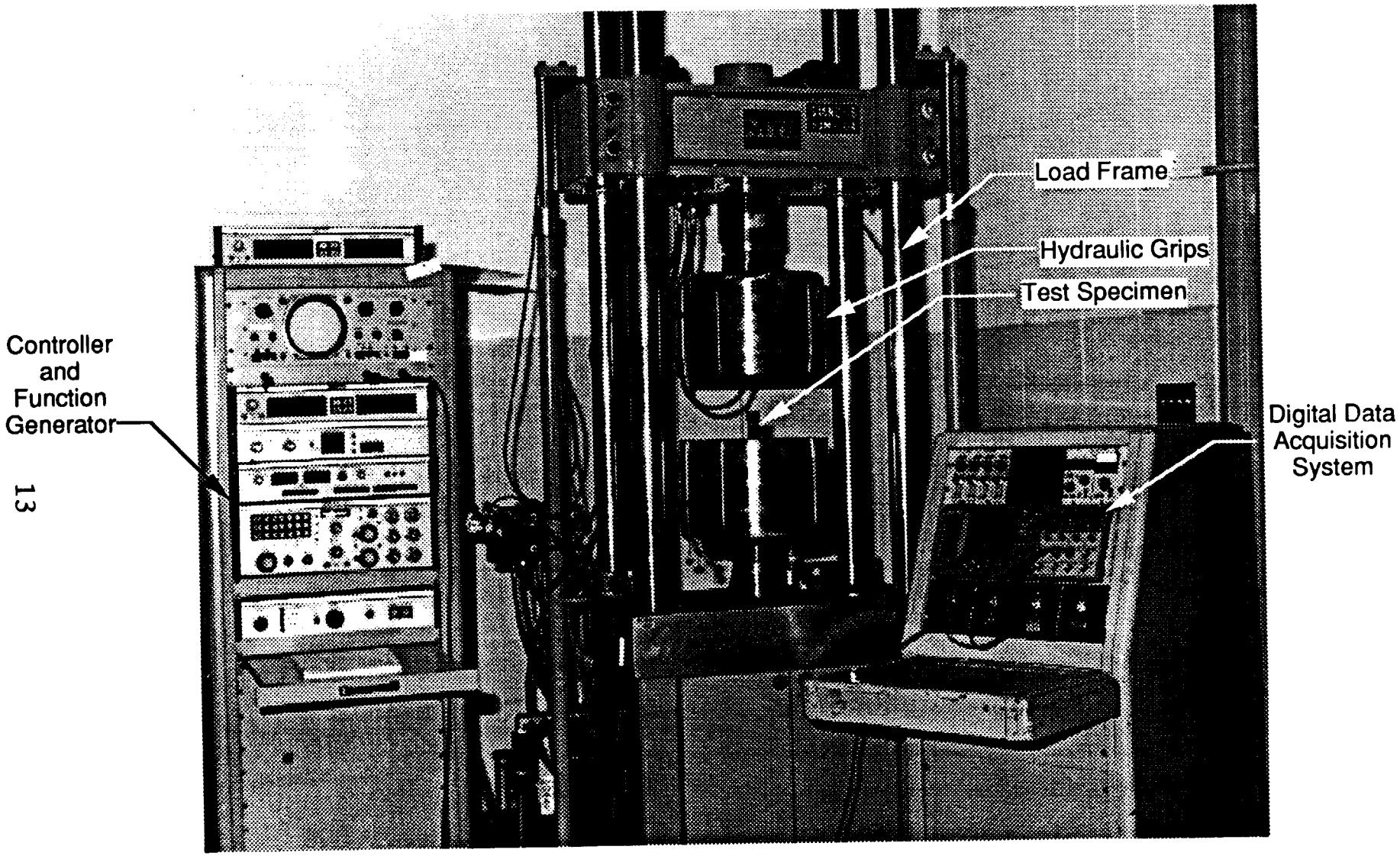

Figure 3. Photograph of the load frame, test specimen, and data acquisition system.

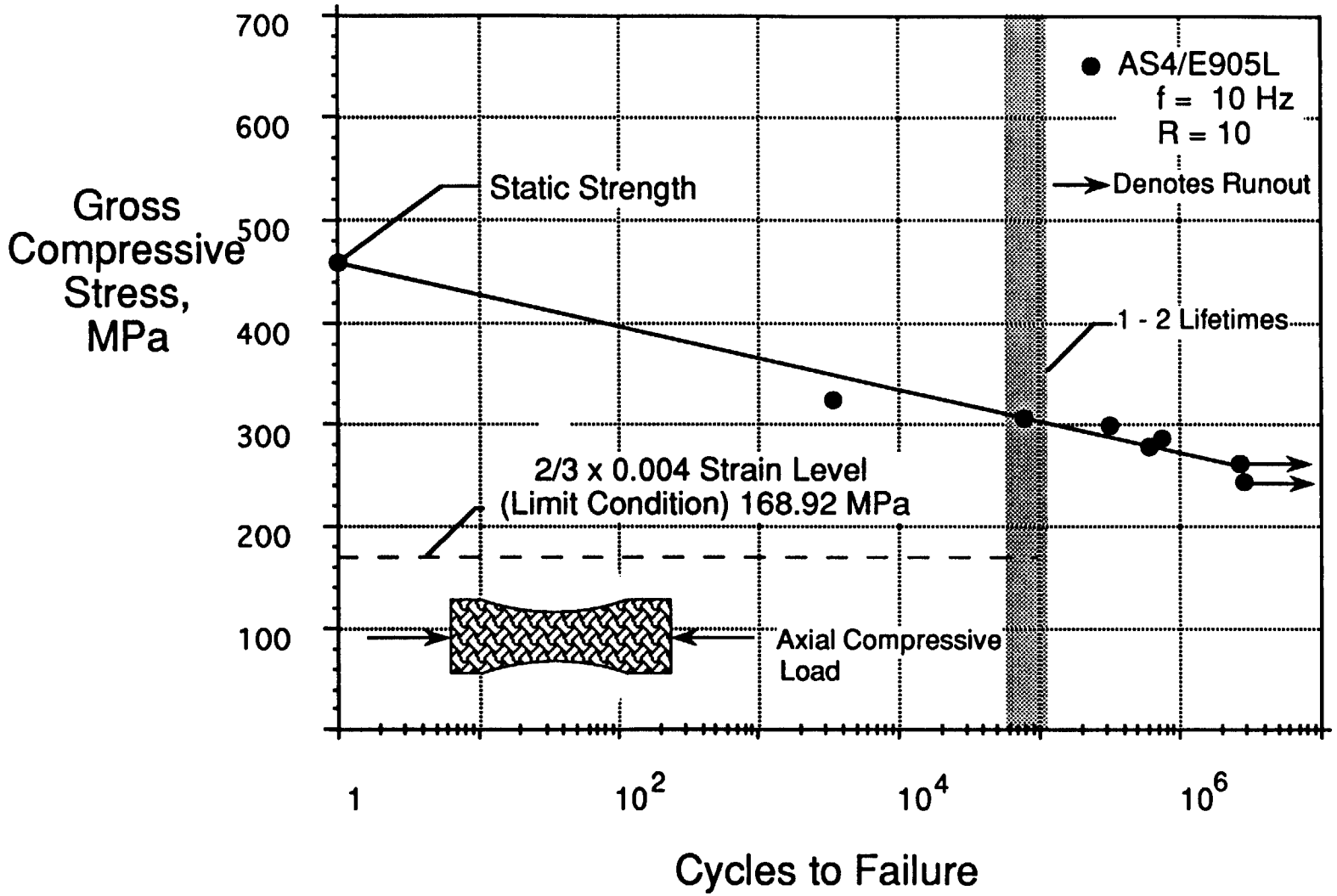

Figure 4. Compression Fatigue of 3D Braids.

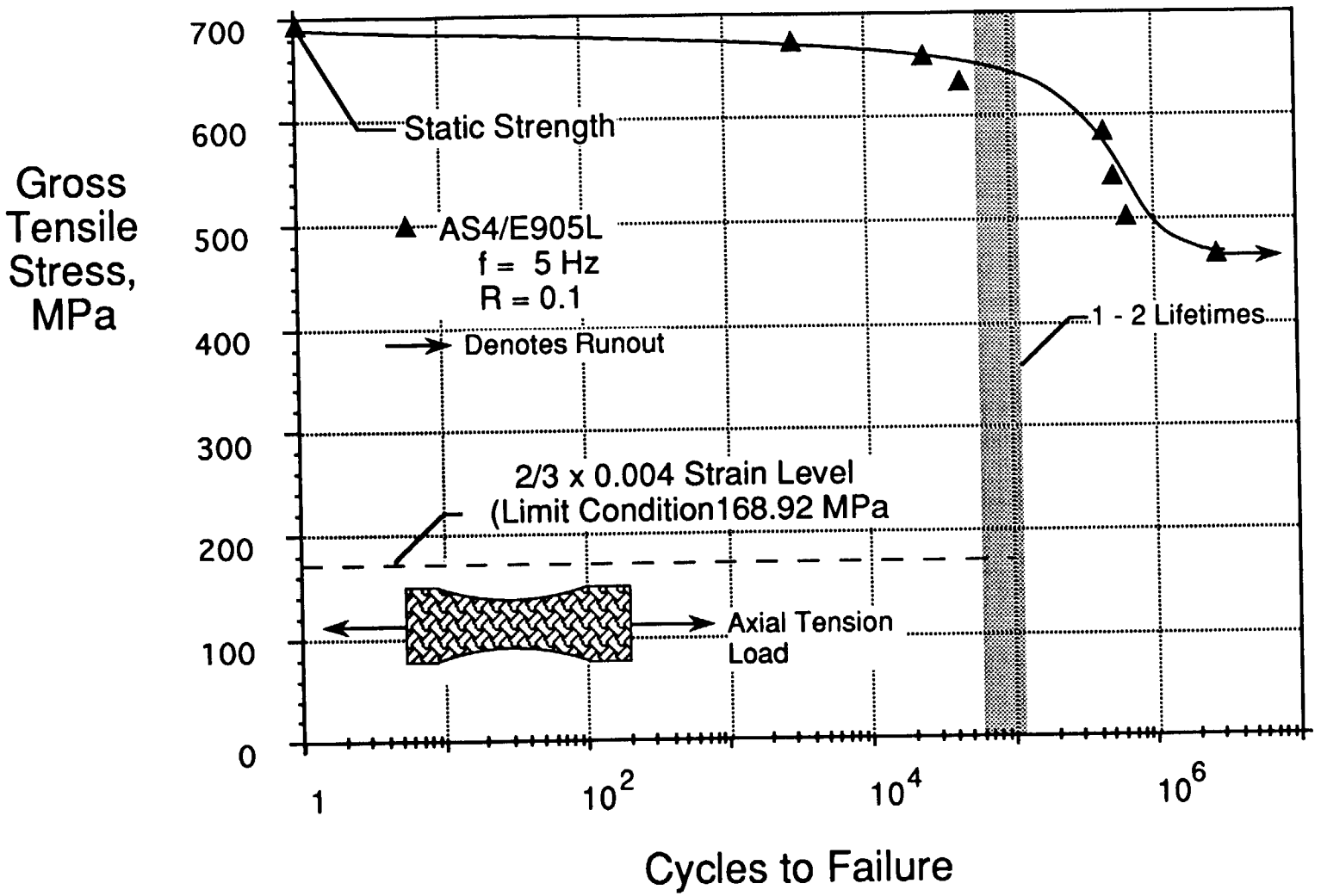

Figure 5. Tension Fatigue of 3D Braids.

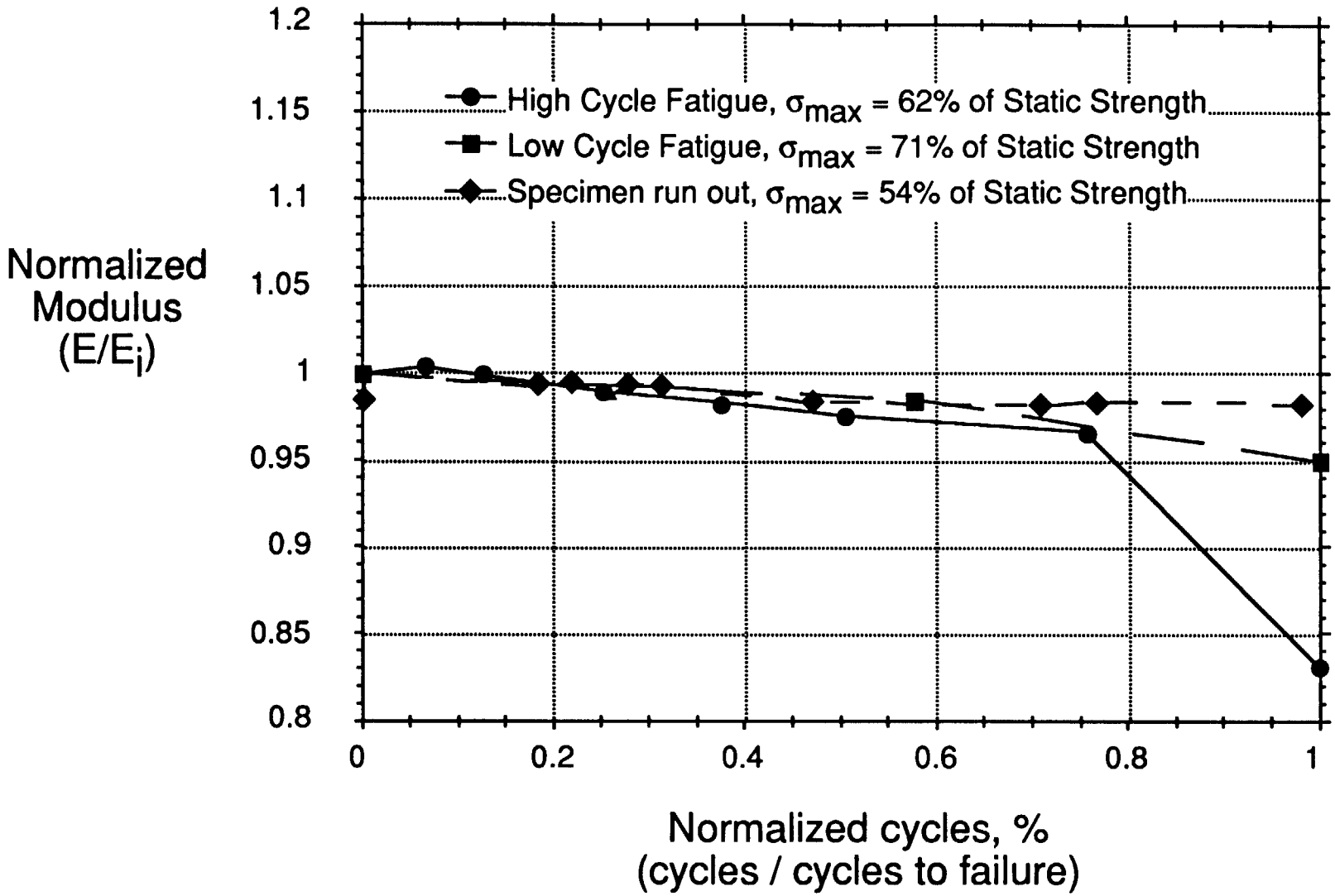

Figure 6. Normalized Compression Modulus -vs- Normalized Life
High Cycle, Low Cycle, Run-out Fatigue.

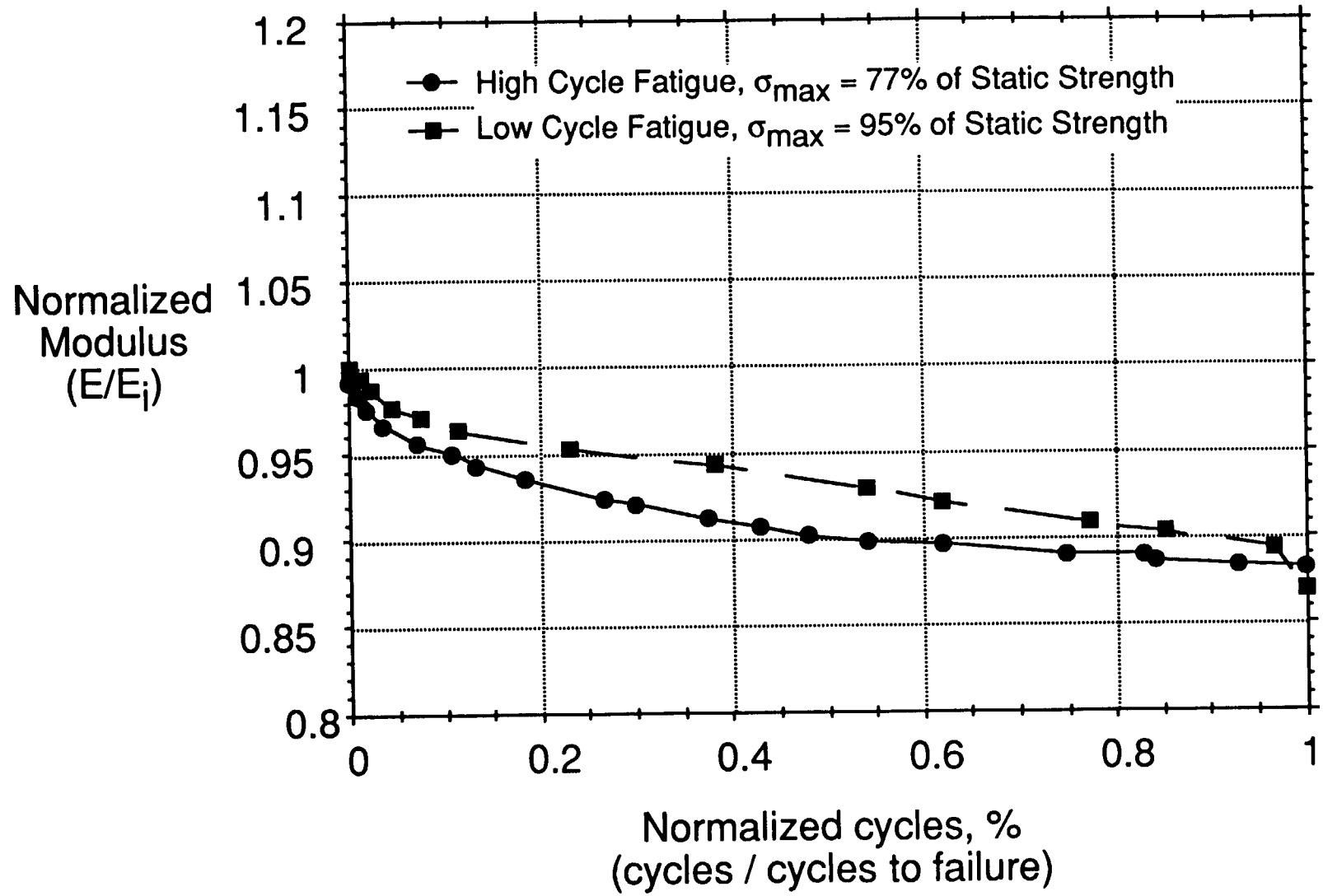

Figure 7. Normalized Tension Modulus -vs- Normalized Life
High Cycle, Low Cycle Fatigue.

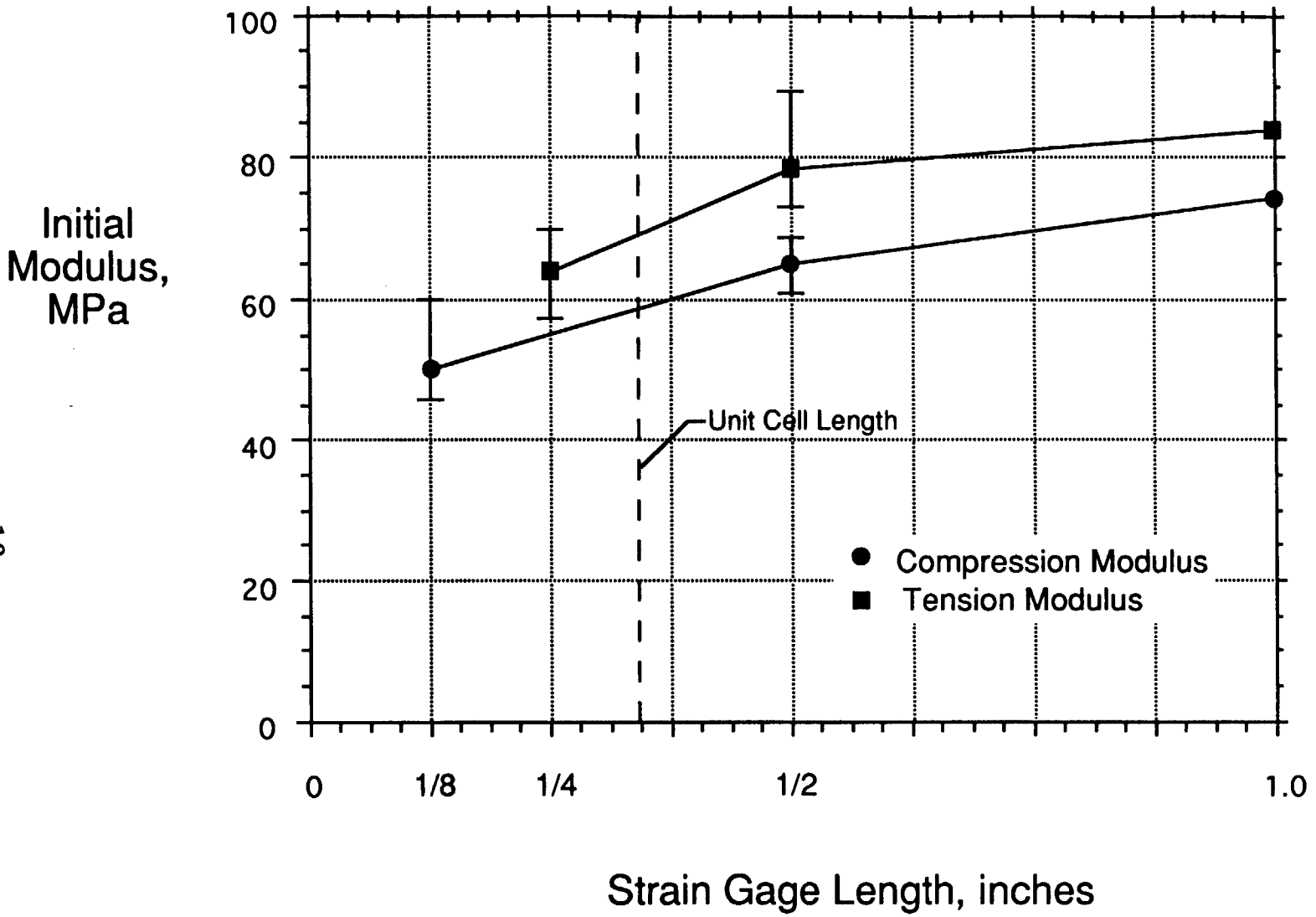

Figure 8. Effect of Strain gage Length on Elastic Modulus.

REPORT DOCUMENTATION PAGE

Form Approved
OMB No. 0704-0188

1. AGENCY USE ONLY *(Leave blank)*	2. REPORT DATE	3. REPORT TYPE AND DATES COVERED
	August 1992	Contractor Report

4. TITLE AND SUBTITLE
Tension and Compression Fatigue Response of Unnotched 3D Braided Composites

5. FUNDING NUMBERS
C NAS1-19000
WU 505-63-50-04

6. AUTHOR(S)
M. A. Portanova

7. PERFORMING ORGANIZATION NAME(S) AND ADDRESS(ES)
Lockheed Engineering & Sciences Company
144 Research Drive
Hampton, VA 23666

8. PERFORMING ORGANIZATION REPORT NUMBER

9. SPONSORING / MONITORING AGENCY NAME(S) AND ADDRESS(ES)
National Aeronautics and Space Administration
Langley Research Center
Hampton, VA 23681

10. SPONSORING / MONITORING AGENCY REPORT NUMBER
NASA CR-189678

11. SUPPLEMENTARY NOTES
Langley Technical Monitor: Charles E. Harris

12a. DISTRIBUTION / AVAILABILITY STATEMENT
Unclassified-Unlimited
Subject Category 24

12b. DISTRIBUTION CODE

13. ABSTRACT *(Maximum 200 words)*

The unnotched compression and tension fatigue response of a 3-D braided composite was measured. Both gross compressive stress and tensile stress were plotted against cycles to failure to evaluate the fatigue life of these materials. Damage initiation and growth was monitored visually and by tracking compliance change during cyclic loading. The intent was to establish by what means the strength of a 3-D architecture will start to degrade, at what point will it degrade beyond an acceptable level, and how this material will typically fail.

14. SUBJECT TERMS
3-D braided composite; Fatigue testing; Unnotched; Damage initiation; Damage growth; Stiffness loss

15. NUMBER OF PAGES
19

16. PRICE CODE
A03

17. SECURITY CLASSIFICATION OF REPORT	18. SECURITY CLASSIFICATION OF THIS PAGE	19. SECURITY CLASSIFICATION OF ABSTRACT	20. LIMITATION OF ABSTRACT
Unclassified	Unclassified		